Localization on Snowflake Domains

Britta Daudert

Department of Mathematics

University of California

Riverside, CA 92521–0135

e-mail address: *britta@math.ucr.edu*

Michel L. Lapidus

Department of Mathematics

University of California

Riverside, CA 92521–0135

e-mail address: *lapidus@math.ucr.edu*

Abstract

The geometric features of the square and triadic Koch snowflake drums are compared using a position entropy defined on the grid points of the discretizations (pre-fractals) of the two domains. Weighted graphs using the geometric quantities are created and random walks on the two pre-fractals are performed. The aim is to understand if the existence of narrow channels in the domain may cause the 'localization' of eigenfunctions.

1   Introduction

The term fractal is defined very loosely [F]. Here are just some ways of characterizing a fractal set F:

- F has a fine structure, i.e., detail on an arbitrary small scale.

- F is too irregular to be described in traditional geometric language, both locally and globally.

- Often, F has some form of self-similarity (maybe strict, approximate or statistical).

- Usually, the fractal dimension of F (defined in some way) is greater than its topological dimension.

- In most cases, F is defined in a very simple way (e.g., recursively).

In short, fractals are objects with irregular geometry. Such objects can be found everywhere in nature, the most obvious example being that of a tree structure. The **vibrational** properties of fractals are of great interest. Questions that arise naturally are, for example:

- Why are waves damped much more by fractal rather than by smooth coastlines?

- How can we explain the vibrational properties of glass?

- Why does fractal foliage of trees provide such strong resistance to the wind?

All these questions are largely unanswered. Fractal geometry is a means to describing strongly irregular objects and questions like the ones mentioned above have played and continue to play an important role in the development of the subject. The main idea is to use strongly irregular but **deterministic** objects as a good approximation to the fractal. If the physical properties of the object of study are related to the character of the geometry, these deterministic approximations prove to be a good source of information.

1.1 Fractal Drums

A fractal drum is the simplest example of a surface fractal resonator. It is a flat surface bounded by a fractal frontier.

Figure 1: An approximation to the triadic Koch Snowflake domain
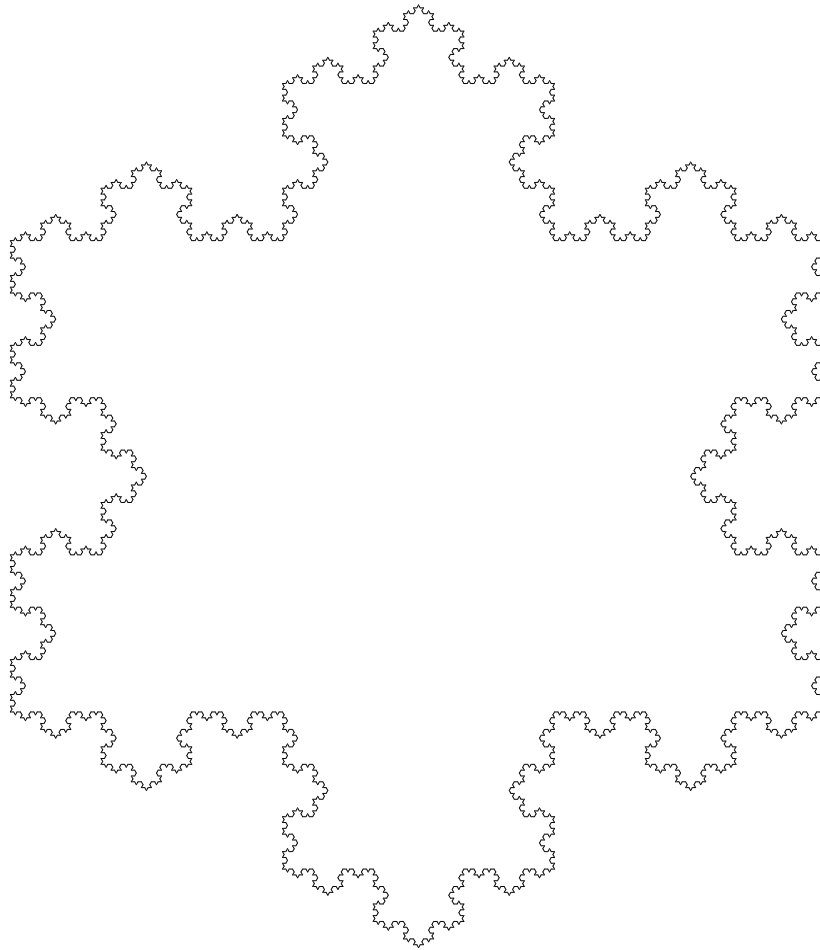
1.2 Vibrational properties of fractal drums

The vibrational properties of these structures are of great theoretical and practical interest [Be1], [Be2], [BroCa], [L1], [L2], [L3], [LNRG], [LP], [Sa2], [EveRRPS], [SG], [SGM].

An extensive amount of experimental work on the study of waves or harmonic oscillations carried by fractals has been done by the physicist B. Sapoval and his collaborators [SG], [SGM]. The **fractal drum** in their experiments consisted of a stainless steel sheet with the boundary etched in the pattern of a square Snowflake. A soap bubble deposited on this object was excited to low frequency vibrations by a loudspeaker situated above the fractal drum. Their results showed that the wave motion is strongly damped by the fractal boundary and that localization may occur. Sapoval attributed this localization to the existence of narrow channels in the geometry of the square domain. This phenomenon was not observed on the triadic Snowflake domain.

In *Snowflake harmonics and computer graphics: numerical computation of spectra on fractal drums* [LNRG], the authors numerically estimated the first 50 eigenvalues and eigenvectors of the triadic Snowflake domain and tested graphically the results and conjectures concerning the boundary behavior of the gradient of the eigenfunctions.

Some mathematical work has been done to confirm Sapoval's results. Recently, M. L. Lapidus and M. Pang [LP] have studied the boundary behavior of the Dirichlet Laplacian eigenfunctions and their gradients on a class of planar domains with fractal boundary, including the (triangular and square) Koch Snowflake domains, as well as their polygonal approximations. One of their main results, specialized to the Koch Snowflake domain, states that the magnitude of the gradient of the first eigenfunction (or 'first harmonic') 'blows up' at infinitely many boundary points, i.e., the membrane of the Koch snowflake drum exhibits 'infinite stress' near such points. Physically, this corresponds to a strong damping phenomenon.

In this paper, we develop a new approach to investigate localization phenomena on fractal drums: the discretizations of the square and triadic Snowflake are considered as weighted graphs. The weight is assigned to an edge in such a way that it reflects certain geometric

properties of the two nodes connected by that edge. The development of random walks initiated in different geometric regions are compared and analyzed.

2 Measures of localization

The main problem when studying the localization of the eigenmodes is to define a suitable notion of localization. What do we mean when talking about localization of an eigenfunction? A function on an unbounded domain is said to be localized if it has compact support or if it is exponentially localized but a generally accepted notion of localization on bounded domains is still missing. In fact, we note that due to the ellipticity of the underlying equation, there cannot exist any Dirichlet eigenfunction that vanishes on a nonempty open subset of the domain [Ev].

2.1 The square and triangular Koch prefractals

The square and triangular prefractals are defined recursively by repeatedly applying the corresponding generators. It was proved that the sequence of square and triangular prefractals converge to the corresponding fractals and that the sequences of the individual eigenvalues of the prefractals converge to the eigenvalues of the actual fractals. Thus, the study of the eigenfunctions on these approximations should give a good insight into the behavior of the eigenfunctions on the true fractals.

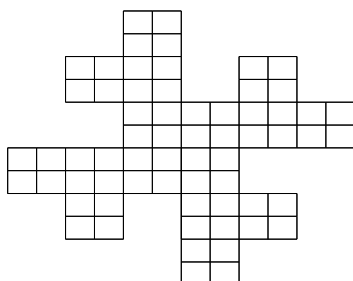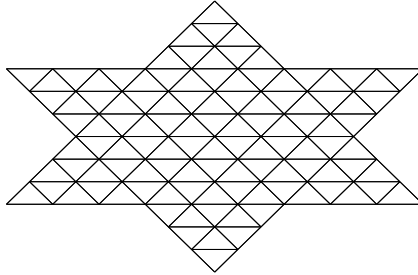Figure 2: Square Snowflake Prefractal

Figure 3: Triadic Snowflake Prefractal

2.2 Localization measures

Some eigenmodes on the square Koch prefractal show confinement to small regions of the membrane. On triadic Koch prefractals, however, no such 'localization' is observed. Sapoval attributed the experimental localization he observed to the effects of

1. Damping

2. The existence of 'narrow paths' in the geometry of the structure.

Figure 4: Eigenfunction 27
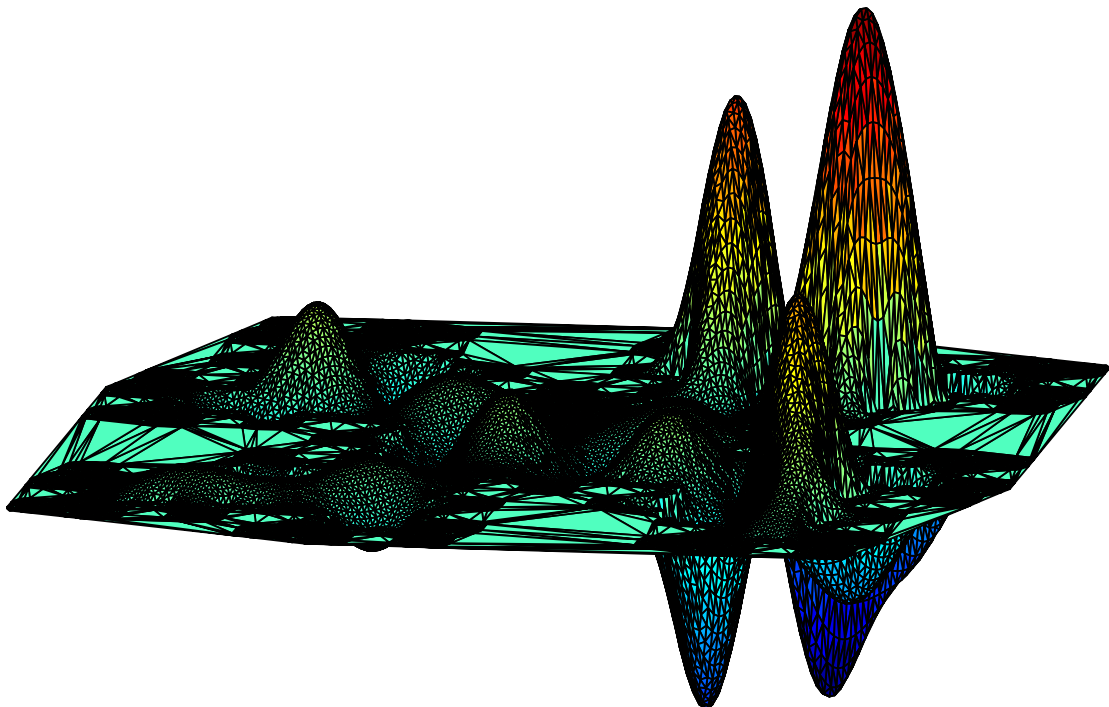
The following quantities were introduced in the literature in an attempt to qualitatively describe localization of functions (Ψ) on bounded domains:

1) *Participation Ratio* $V_p(\Psi)$ [We]

The Participation Ratio is defined as $PR(\Psi) = \frac{1}{\int_D |\Psi(x)|^4 dx}$. It can be regarded as the effective number of nodes participating in the function Ψ with significant weight.

2) *Participation Volume* $V_p(\Psi)$ [BeDe]

The Participation Volume is a measure of the effective number of 'atoms' of an 'ensemble' participating in a vibration on a domain D: $V_P(\Psi) = \frac{\left(\int_D \left(|\Psi(x)|^2 dx\right)\right)^2}{\int_D |\Psi(x)|^4 dx}$. $V_P(\Psi)/V$, where V is the volume of the domain D, can be used to distinguish between '**extended**' (non-localized states) and '**exponentially localized states**' (the amplitude decays exponentially for sufficiently large distances from some central point).

In this paper we use the Participation Ratio in conjunction with suitable notions of diameter and entropy to investigate localization phenomena on the square and triadic Snowflake domains.

3 The Geometry of the Square and Triadic Snowflake Domains

How can we describe the existence of narrow channels in the geometry of the square Snowflake? We will attempt to classify different regions by defining the following six distances for an interior grid point (x, y):

Let $dh_+(x, y)$, $dh_-(x, y)$ be the right and left horizontal distances of (x, y) from the boundary and dv_+, dv_- be the up and down vertical distances of (x, y) from the boundary. Now define

- $dh(x, y) = dh_+(x, y) + dh_-(x, y)$

- $dv(x, y) = dv_+(x, y) + dv_-(x, y)$.

Using $dh(x, y)$ and $dv(x, y)$, one can distinguish between three geometrically different regions of the domain in question:

1. **'The Grottos'**: Regions confined in both directions.

   For example, some gridpoints close to the boundary have $dv \approx dh$ taking small values.

2. **'The Canyons'**: Narrow channels.

   Points lying in those regions have either $dv \ll dh$ or $dh \ll dv$.

3. **'The Prairies'**: Relatively unconfined regions.

   Some points in the center of the domain, for example, have $dv, dh \approx 1/2$ and hence should be considered as lying in an unconfined region.

Remark: Note that points in region one as well as points in region three have $dv \approx dh$. Since the ultimate goal is to define a measure distinguishing between the three different geometric regions, it is clear that plainly using $dh(x, y)$ and $dv(x, y)$ will not do.

We thus define the following three quantities:

1. $\partial_{min}(x, y) = \min \{dh_+(x, y), dh_-(x, y), dv_+(x, y), dv_-(x, y)\}$

2. $\partial_{rat}(x, y) = \min \{\frac{dh(x,y)}{dv(x,y)}, \frac{dv(x,y)}{dh(x,y)}\}$

3. $\partial_{rat}^{min}(x, y) = \partial_{rat}(x, y) * \partial_{min}(x, y)$.

Note that for interior grid points in $SQ(L, R)$, $(L > 0)$ with grid size $H_{SQ(L,R)} = (\frac{1}{2})^{2L+R}$, we have

1. $\partial_{min} \in [H_{SQ(L,R)}, 1/4]$

2. $\partial_{rat} \in [2H_{SQ(L,R)}, 1]$

3. $\partial_{rat}^{min} \in [2(H_{SQ(L,R)})^2, 1/4]$.

For interior grid points in $T(L, R)$, $(L > 0)$ with grid size $H_{T(L,R)} = (\frac{1}{3})^{L+R}$, we have

1. $\partial_{min} \in [\frac{\sqrt{(3)}}{2}H_{T(L,R)}, \frac{1}{\sqrt{3}}]$

2. $\partial_{rat} \in [\frac{2}{\sqrt{3}}H_{T(L,R)}, 1]$

3. $\partial_{rat}^{min} \in [(H_{T(L,R)})^2, \frac{1}{\sqrt{3}}]$.

Let us consider the properties of ∂_{rat} and ∂_{rat}^{min} in the three different regions:

Properties of ∂_{rat}

- if (x, y) **lies in a grotto**,

  then $dv \approx dh$ and $\partial_{rat}(x, y) \approx 1$.

- if (x, y) **lies in a canyon**,

  then $dv \ll dh$ or $dh \ll dv$ and $\partial_{rat}(x, y)$ is small.

- if (x, y) **lies in a prairie**,

  then $dv \approx dh$ and $\partial_{rat}(x, y) \approx 1$.

Properties of ∂_{rat}^{min}

Let us assume that the fractal and refinement levels are not both zero.

- if (x, y) **lies in a grotto**,

  then $\partial_{rat}^{min}(x, y)$ $(\approx \partial_{min}(x, y))$ is small.

- if (x, y) **lies in a canyon**,

  then $\partial_{rat}^{min}(x, y)$ $(\approx (\partial_{min}(x, y))^2)$ is very small.

- if (x, y) **lies in a prairie**,

  then $\partial_{rat}^{min}(x, y)$ $(\approx \partial_{min}(x, y))$ is relatively large.

Let us now compare the features of $\partial_{rat}^{min}(x,y)$ on the two domains:

$\partial_{rat}^{min}(x,y)$	Square Snowflake	Triadic Snowflake
Maximum	0.25	0.4208
Minimum	0.001	0.0002
Minimum/Maximum	$4 * 10^{-3}$	$4.75 * 10^{-4}$
Median	0.0156	0.0216
Mean	0.0332	0.0724
Standard Deviation	0.0467	0.0967
Median/Maximum	0.0624	0.0513
Mean/Maximum	0.1328	0.172

Table 1: Comparison of $\partial_{rat}^{min}(x,y)$ at $(L,R) = (2,2)$

Note from table 1 that the maximum of ∂_{rat}^{min} on the square Snowflake is $\frac{1}{4}$ while it is $\frac{1}{\sqrt{3}}$ on the triadic Snowflake. The minimum value of ∂_{rat}^{min} on the interior of the triadic domains is smaller than that on the square domain, while the mean value of ∂_{rat}^{min} is smaller on the square Snowflake.

We find that in both domains, the mean value of ∂_{rat}^{min} lies closer to the minimum value of ∂_{rat}^{min} than to the maximum value. Together with the low medians (only 6.24% of the maximum on the square, 5.13% of the maximum on the triadic domain), this means that a lot of points on either domain have a relatively small ∂_{rat}^{min} value. The relative mean value of ∂_{rat}^{min} is higher on the triadic Snowflake due to the triangular geometry. At refinement and fractal level equal to two, we find that the difference between the maximum and the mean value lies at about 0.2168 for the square Snowflake and at about 0.4206 for the triadic Snowflake. The differences between minimum value and mean value lie at about 0.0322 and 0.0722, respectively.

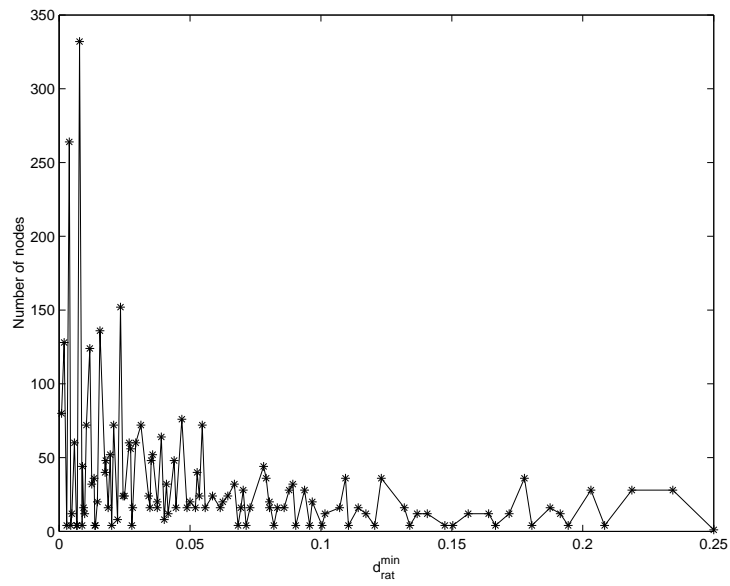Figure 5: Square Snowflake d_{rat}^{min} distribution

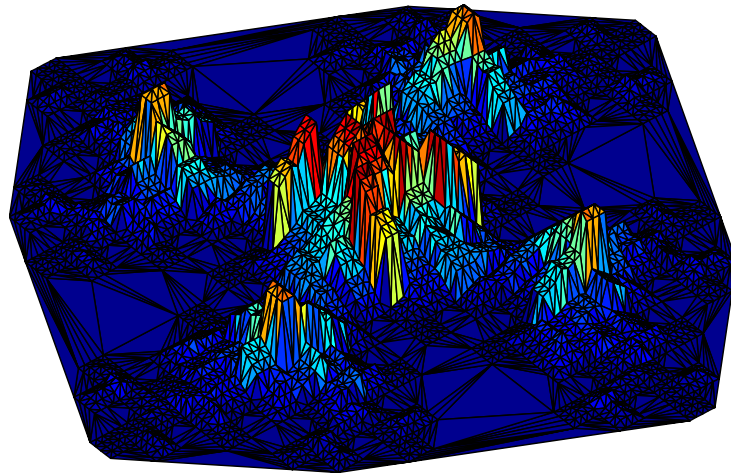Figure 6: Square Snowflake d_{rat}^{min} surface plot

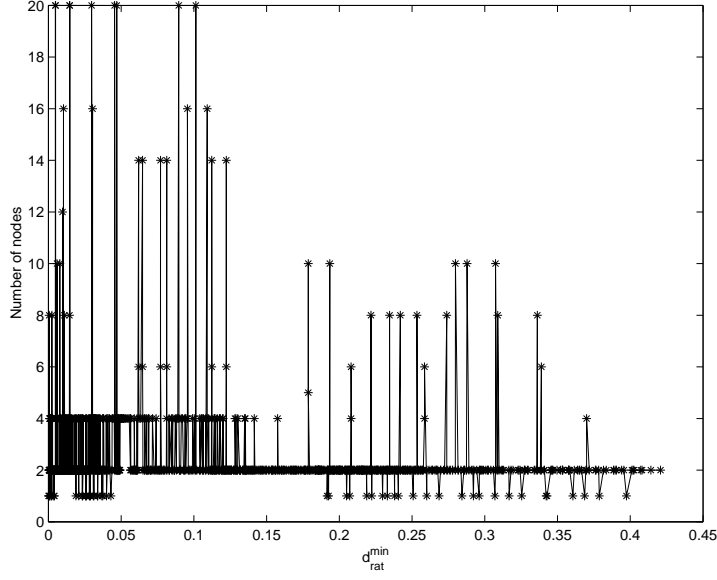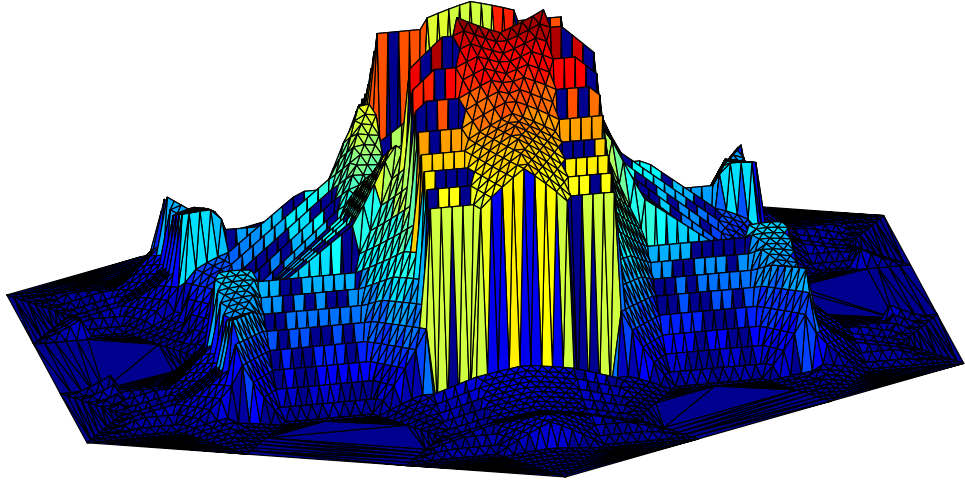Figure 7: Triadic Snowflake d_{rat}^{min} distribution

Figure 8: Triadic Snowflake d_{rat}^{min} surface plot

4 Position Entropy

In this section, we will use ∂_{rat}^{min}, defined in the previous section, to define a probability distribution $P_{x,y}(\partial)$ on each node of our discretization. This probability distribution is used to define a position entropy $S(x, y)$ at each vertex.

For (x, y), a grid point of the discretization of the snowflake domain, let

$$P_{(x,y)}(\partial) := percentage \quad of \quad neighbours \quad of \quad node \quad (x, y) \quad with \quad \partial_{rat}^{min} = \partial. \quad (1)$$

Then $\sum_\partial P_{(x,y)}(\partial) = 1$ for each node (x, y) and hence, P defines a probability distribution. Now let

$$S(x, y) := -\sum_\partial P_{(x,y)}(\partial) \ln \left(P_{(x,y)}(\partial) \right). \quad (2)$$

This entropy gives information about the disorder in the values of ∂_{rat}^{min} at neighboring points of the vertex in question. The more variation in ∂_{rat}^{min}, the larger the value of $S(x, y)$ will be.

Table 2: Comparison of Position Entropy at $(L, R) = (2, 2)$

Position Entropy	Square Snowflake	Triadic Snowflake
Maximum	0.0157	0.0238
Minimum	$2.63 * 10^{-14}$	$1.28 * 10^{-10}$
Minimum/Maximum	$1.675 * 10^{-12}$	$5.378 * 10^{-9}$
Median	0.0085	0.0114
Mean	0.0089	0.0114
Standard Deviation	0.0041	0.0059
Median/Maximum	0.5414	0.47899
Mean/Maximum	0.5668	0.47899

Comparing our two domains at $(L, R) = (2, 2)$, we find from table 2 that the mean and median values are the same on the triadic Snowflake and close to each other on the square Snowflake, and in both domains, they lie closer to the maximum value of S than to the minimum value. This means that most of the points on either domain have a relatively large entropy values, i.e., the values of ∂_{rat}^{min} in the neighborhood of those points are not evenly distributed. The relative median and mean of S are higher on the square Snowflake. At refinement and fractal level equal to 2, we find that the difference between the maximum and the mean value lies at about 0.28 for the square Snowflake and at about 0.38 for the triadic Snowflake. The differences between minimum value and mean value lie at about 0.83 and 0.95, respectively.

In summary, we can say that the relative mean and median of the entropy found on the square domain are significantly larger (about 10%). The ∂_{rat}^{min} characteristics of both domains are similar but we find a slightly higher (1%) relative median and a lower mean (about 4%) on the square Snowflake.

We refer to figures 9–12 for the distribution and the surface plot of the square and triadic Snowflake domains.

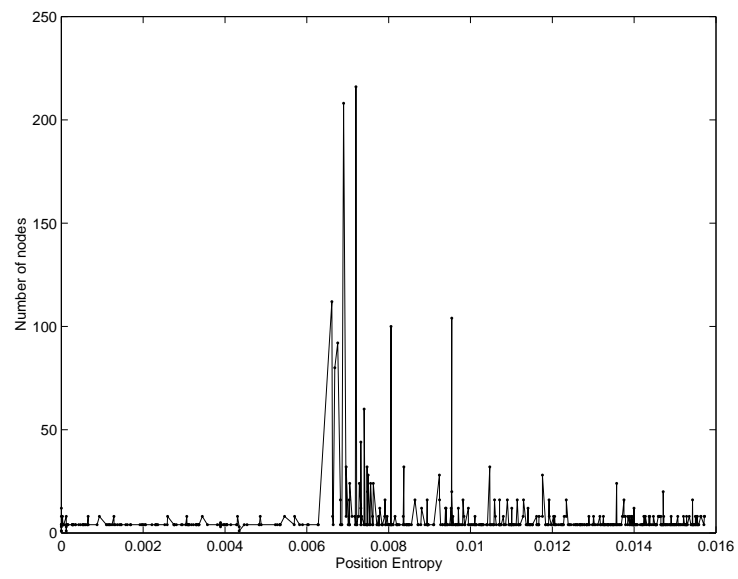Figure 9: Square Snowflake Position Entropy distribution

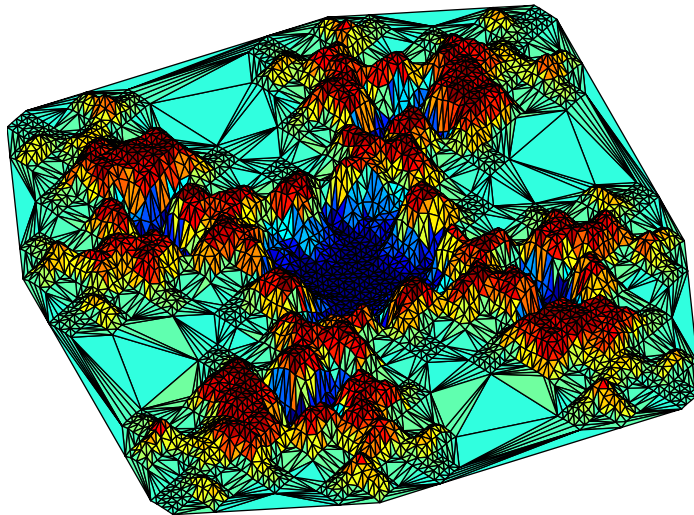Figure 10: Square Snowflake Position Entropy surface plot

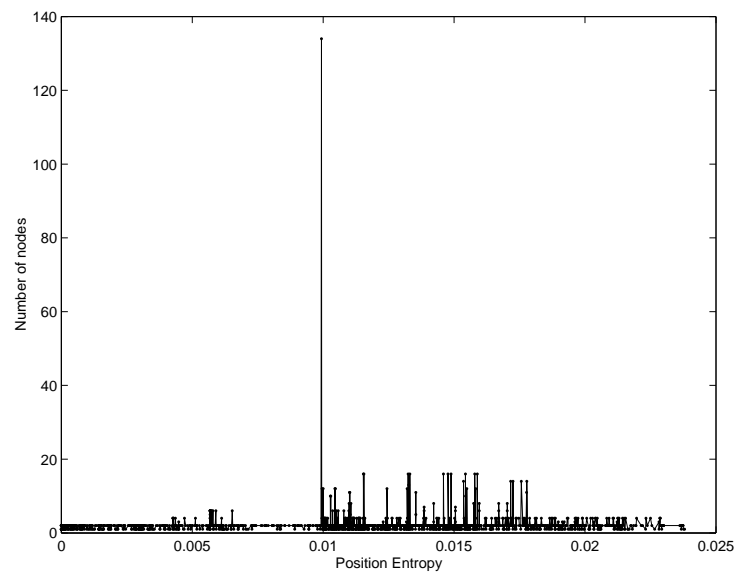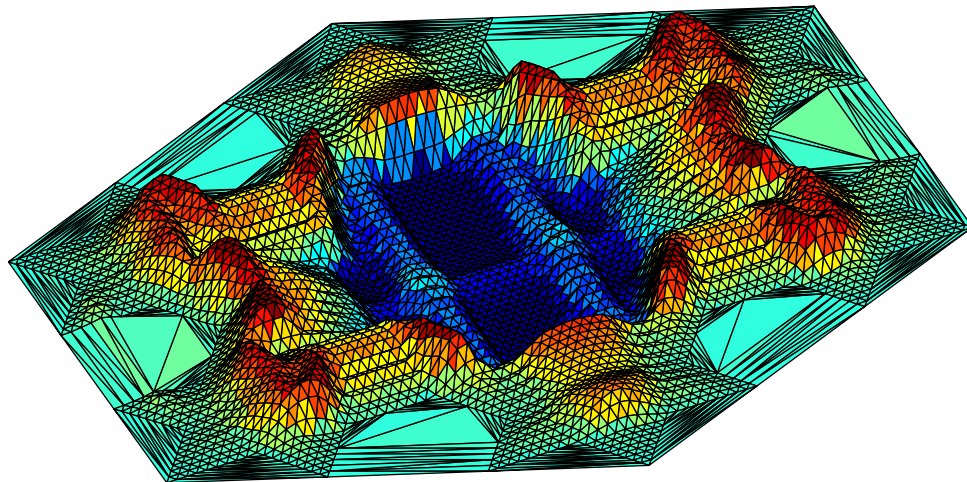Figure 11: Triadic Snowflake Position Entropy distribution

Figure 12: Triadic Snowflake Position Entropy surface plot

5 Random Walks on Discretizations of Snowflake Domains

In this section, we will study diffusion (random walks) on discretization graphs of the Snowflake domains. This work is inspired by I. Simonsen et. al. [SiErMaSn], [Si]. In their papers, these authors use diffusion on networks to derive a master equation whose analysis reveals information about the large-scale structure of the network. By performing random walks governed by the underlying master equation on the two Snowflake domains, we hope to gain useful insights into their geometric properties and an understanding of why localization is favored by the Square domain. This will provide a new way to investigate localization for domains with fractal boundaries. This study relies in part on the notions of distance and entropy introduced earlier in this paper (see Sections 3 and 4).

The nodes of the discretizations represent the vertices and the edges are given by the neighbor relations. The path taken by our random walkers will be influenced by the geometric features of the domain:

The edge e_{ij}, going from vertex v_i to vertex v_j is assigned a weight inversely proportional to $1 - \partial_{rat}^{min}(j)$, where ∂_{rat}^{min} is normalized such that it takes values in $[0, 1]$. Hence, edges where node v_j lies in a Grotto have large weights assigned, edges where node v_j lies in a Canyon have even larger weights (close to 1) assigned, while edges with node v_j lying in a Prairie have relatively small weights assigned, i.e., the weights are assigned to the edges in such a way that a random walker is strongly encouraged to move to regions with distances that describe narrow channels, then to regions confined in both directions, and lastly to unconfined regions. If localization is caused by the existence of narrow channels, as predicted by Sapoval, we expect to see some kind of congregation of the walkers in those areas of the domain that are characterized by predominantly large weights.

We start our random walk by placing a large number of random walkers onto the vertices of the network. At each time step, these walkers are allowed to move between adjacent

vertices. The edge, out of the possible outgoing ones, a walker chooses to move along is picked at random with a probability equal to the weight assigned to this edge.

We define the adjacency matrix A as follows:

$$A_{ij} = \begin{cases} 1, & \text{if } \quad nodes \quad v_i \quad and \quad v_i \quad are \quad neighbors \\ 0, & else. \end{cases}$$

Note that the weight matrix $W = \{w_{ij}\}_{i,j} = \{A_{ij}(1 - \partial_{rat}^{min}(j))\}$ is non-symmetric.

5.1 The Master Equation

Let nv be the number of vertices in the discretization and N be the number of participating random walkers. Let the number of walkers situated at node v_i at time t be denoted by $N_i(t)$. Then the fraction of walkers at this node at time t is

$$\eta_i(t) = \frac{N_i(t)}{N}. \tag{3}$$

Since the total number of random walkers is preserved at each time, we have $\sum_i \eta_i(t) = 1$.

The change in the walker density of a vertex v_i during one time step equals the difference between the relative number of walkers entering and leaving the same vertex over the time interval. In mathematical terms we can write

$$\eta_i(t+1) = \eta_i(t) + J_i^-(t) - J_i^+(t), \tag{4}$$

where $J_i^\pm(t)$ denote the relative number of walkers entering (-) and leaving (+) vertex v_i.

The value of $J_i^+(t)$ depends on the **strength** St_i of node v_i i.e., the total number of outgoing weights $St_i = \sum_{j \in Neigh_i} w_{ij}$, where $Neigh_i$ denotes the set of neighbors of node v_i. Similarly, the value of $J_i^-(t)$ depends on the total number of incoming weights $\sum_{j \in Neigh_i} w_{ji}$. The

fraction of outgoing walkers from vertex v_i (a current) per unit weight is thus

$$c_i(t) = \frac{\eta_i(t)}{\sum_{j \in Neigh_i} w_{ij}}. \tag{5}$$

Hence, $c_i(t)$ is the weighted walker density per link of node v_i at time t.

The edge current on the directed edge from vertex v_i to vertex v_j is then given by

$$C_{ij}(t) = w_{ij}c_i(t) = w_{ij}\frac{\eta_i(t)}{\sum_{k \in Neigh_i} w_{ik}}. \tag{6}$$

Notice that the term

$$\frac{w_{ij}}{\sum_{k \in Neigh_i} w_{ik}}$$

is the probability of a walker moving from vertex v_i to vertex v_j.

The relative number J_i^+ of outgoing walkers from node v_i at time t is given by

$$J_i^+(t) = \sum_{j \in Neigh_i} C_{ij} \tag{7}$$

and the relative number J_i^- of incoming walkers to node v_i at time t is given by

$$J_i^-(t) = \sum_{j \in Neigh_i} C_{ji}. \tag{8}$$

It is easy to verify that $J_i^+(t) = \eta_i(t)$. This expresses the fact that all walkers leave their respective vertices at each time step, i.e., no walker stays at the same vertex for more than one time step.

Denoting $\partial_t \eta_i(t) = \eta_i(t-1) - \eta_i(t)$ and substituting the expressions for $J_i^+(t)$ and $J_i^-(t)$ into equation (4), we find

$$\partial_t \eta_i(t) \;=\; \sum_{j \in Neigh_i} C_{ji} - \eta_i(t)$$

$$= \sum_{j \in Neigh_i} \frac{w_{ji}\eta_j(t)}{\sum_{k \in Neigh_j} w_{jk}} - \eta_i(t)$$

$$= \sum_{j \in Neigh_i} T_{ij}\eta_j(t) - \eta_i(t), \tag{9}$$

where

$$T_{ij} := \frac{w_{ji}}{\sum_{k \in Neigh_j} w_{jk}}.$$

This equation can be written in matrix form, as follows:

$$\eta(t+1) = \mathbf{T}\eta(t) \tag{10}$$

Equation (10) is known as the master equation for the random walk process of the underlying network. Further, $\mathbf{T} = \{T_{ij}\}$ is called the transfer matrix. It 'transfers' the walker distribution one step ahead and therefore can be thought of as a time propagator for the process. For some arbitrarily chosen initial state $\eta(0)$, the time development can be obtained by iterations of equation (10), with the result $\eta(t) = \mathbf{T}^{(t)}\eta(0)$. Hence, the eigenvalue spectrum of $\mathbf{T}$ controls the time evolution of the diffusive process.

Due to the fact that our weight matrix is not symmetric, the matrix $\mathbf{T}$ also fails to be symmetric. However, $\mathbf{T}$ is similar to the symmetric matrix $\mathbf{S} = \mathbf{KTK^{-1}}$, where

$$K_{ij} := \begin{cases} \dfrac{\delta_{ij}}{\sqrt{w_{ij}}*\sqrt{\sum_{k \in Neigh_j} w_{jk}}}, & \text{if} \quad w_{ij} \neq 0 \\ 1, & else, \end{cases}$$

and hence

$$(KTK^{-1})_{ij} \;=\; \frac{\sqrt{w_{ii} w_{jj}}}{\sqrt{\sum_{k \in N_i} w_{ik} \sum_{k \in N_j} w_{jk}}}$$

$$= \frac{\sqrt{(1 - \partial_{rat}^{min}(i))(1 - \partial_{rat}^{min}(j))}}{\sqrt{[\sum_{k \in N_i}(1 - \partial_{rat}^{min}(k))][\sum_{k \in N_j}(1 - \partial_{rat}^{min}(j))]}}.$$

$$\tag{11}$$

Therefore, $\mathbf{T}$ is guaranteed to have real eigenvalues and corresponding eigenvectors. It is convenient to sort the eigenvalues in descending order. Furthermore, as a consequence of the Perron–Frobenius theory, the eigenvalue $\lambda_1 = 1$ is simple and the elements of the corresponding eigenvector will all have the same sign.

Physically, the state $\lambda_1 = 1$ corresponds to the stationary state such that $\eta(\infty) \propto \eta^{\mathbf{t}}$, where the diffusive current flowing from node v_i to node v_j is exactly balanced by that flowing from v_j to v_i. Since $|\lambda_k| < 1$ for $k \neq 1$, all modes corresponding to those eigenvalues are decaying. $\lambda_k > 0$ correspond to non-oscillating modes while $\lambda_k < 0$ correspond to states where oscillation will take place over time. The large scale topology of the given network reflects itself in the statistical properties of the eigenvectors η_k [SiErMaSn], [Si].

6   Numerical Work

As shown in the previous section, a random walk on the discretization of the square and triadic Snowflake domains is governed by the master equation $\eta(t) = \mathbf{T}^{(t)}\eta(0)$, where $\eta(t)$ is the distribution of random walkers at time t. In this section, we will discuss numerical simulations of these random walks. Initially, we will place all random walkers at one vertex. By repeatedly applying T to our distribution, we are able to obtain the new walker distributions for each time step. We expect that the dynamics of this system is strongly influenced by the choice of the initial node. Recall that a node lying in a narrow channel is characterized by small ∂_{rat}^{min} and entropy values. Hence, in accordance with the definition of the weight matrix W ($w_{ij} = 1 - \partial_{rat}min(j)$), if narrow channels in the geometry of the square Snowflake exist, we would hope to see a concentration of walkers in the regions where ∂_{rat}^{min} and entropy values are low.

Figure 13: Triadic Snowflake: Position Entropy plus Ratio Distance contour plot
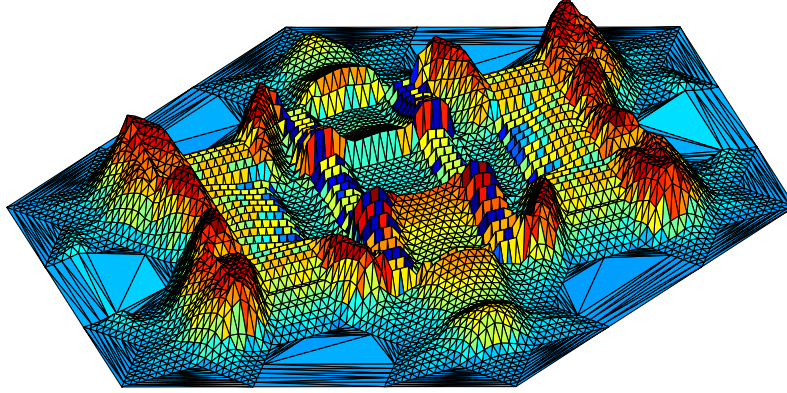
In figure 13, we see a plot of the relative Minimum Ratio Distances added to the relative Position Entropies at each grid point of the Triadic Snowflake. As expected, we see low values close to the boundary. Indeed, random walkers situated here are expected to stay localized in the region. The center part of the Snowflake comprises a medium value square on the left and right of which we find two rectangular discrete low bands and 4 other medium value regions situated north, west, south and east of the center square. In summary, the triadic Snowflake has a relatively big open area of low and medium values in its center. This is not the case for the square Snowflake.

Figure 14: Square Snowflake: Position Entropy plus Ratio Distance contour plot
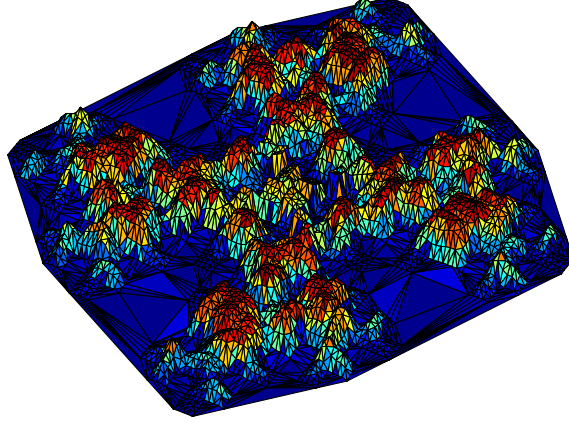
Figure 14 shows a plot of the relative Minimum Ratio Distances added to the relative Position Entropies at each grid point of the square Snowflake. Note that in the center we find relatively high values but, surrounding that center, we find a band of low entropy and distance values. We see four arms of high entropy/distance stretching through parts of the domain almost reaching the boundary. In each of those four arms we can find a small low value basin. The remaining regions between the arms and near the boundary are also characterized by low values. We would expect that a random walk started in any of the basins would stay localized, i.e., that the majority of high/low amplitudes can be found there. If the random walk is initiated in a high altitude region, we would hope to see no such localization. If this were observed, it would indeed indicate that localization really is caused by the existence of narrow channels.

To test this theory, we initially place all random walkers at a point of interest (low entropy/low distance, high entropy/high distance, low entropy/high distance or high entropy/low distance) and then watch the random walk evolve by computing the following quantities at time t:

- the diameter $DIAM(t)$, the furthest distance from the initial node traveled by a random walker during $[0, t]$.

- the Participation Ratio $PR(t) = \frac{1}{\sum_i [\eta_i(t)]^4}$, where $\eta_i(t)$ is the percentage of random walkers at node v_i at time t.

We define high amplitude points at time t as points where $|\eta_i(t)| > (3/4)max(|\eta_i(t)|)$ and compute

- $D_{ha}^{rel}(t)$, the Relative Minimum Ratio Distance of high amplitude points at time t, i.e., $D_{ha}^{rel}(t) = \frac{mean((\partial_{rat}^{min})_{ha}(t))}{max(\partial_{rat}^{min})}$, where $mean((\partial_{rat}^{min})_{ha}(t))$ is the mean of the Minimum Ratio Distances of high amplitude points.

- $S_{ha}^{rel}(t)$, the Relative Position Entropy of high amplitude points at time t, i.e., $S_{ha}^{rel}(t) = \frac{mean(S_{ha}(t))}{max(S)}$, where $mean(S_{ha}(t))$ is the mean of the entropies of high amplitude points.

- $DIAM_{ha}^{rel}(t) = \frac{DIAM_{ha}(t)}{DIAM(t)}$, the Relative Diameter of high amplitude points at time t ($DIAM_{ha}(t)$ denotes the diameter of high amplitude points).

We also keep track of where the walk was started. Since we want to be able to compare values on the two different domains, we will need to compute relative rather than actual values: Instead of listing $\partial_{rat}^{min}(1)$ and $S(1)$, we list $\partial_{rel}(1) = \frac{\partial_{rat}^{min}(1)}{max(\partial_{rat}^{min})}$ and $S_{rel}(1) = \frac{S(1)}{max(S)}$.

The following six figures, numbered 15–20, show some typical plots obtained from our numerical calculation. We would like to point out that there is a lot of variation in the character of the plots: On both domains, the plots of the four quantities look different for different starting nodes but in almost all cases, the four quantities approach an asymptotic limit after about 200 time steps.

Figure 15: Square Snowflake: Random Walk Simulation
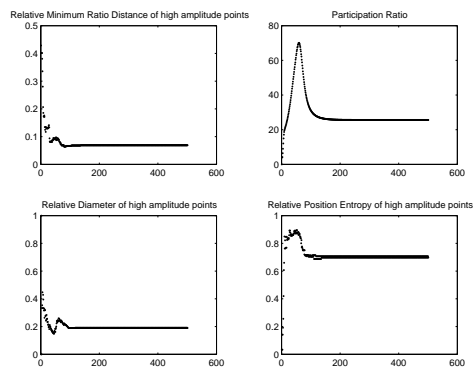

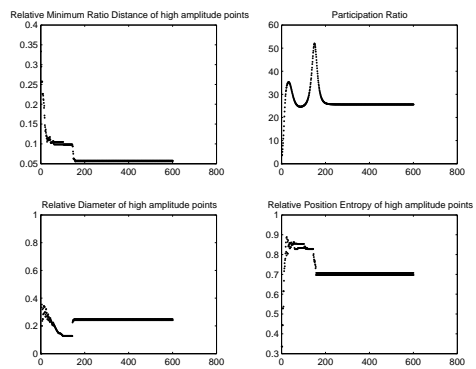Figure 16: Square Snowflake: Random Walk Simulation

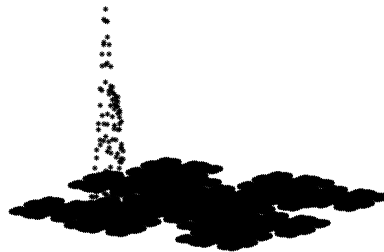Figure 17: Square Snowflake: Random Walk Frame

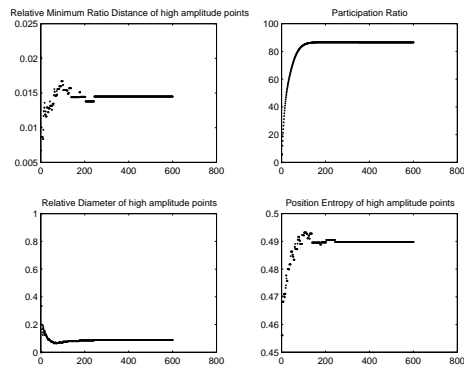Figure 18: Triadic Snowflake: Random Walk Simulation

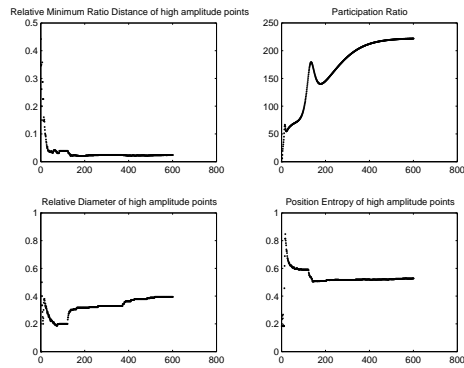Figure 19: Triadic Snowflake: Random Walk Simulation

Figure 20: Triadic Snowflake: Random Walk Frame
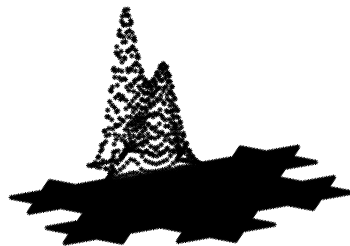
Figure 19 shows a simulations that takes more than 200 time steps for the values to approach the steady state.

Let us look at some random walks started at low entropy/low ∂_{rat}^{min} nodes on both domains.

Table 3: **Square Snowflake** ($\partial_{rat}^{min}(1)$ decreases)

$\partial_{rel}(1)$	$S_{rel}(1)$	$PR(\infty)$	$DIAM(\infty)$	$D_{ha}^{rel}(\infty)$	$S_{ha}^{rel}(\infty)$	$DIAM_{ha}^{rel}(\infty)$
0.4572	$8.21 * 10^{-3}$	25.6456	0.9254	0.0559	0.707	0.5829
0.3216	0.12	25.5995	0.9512	0.0667	0.69	0.54
0.3124	0.146	25.5997	0.9071	0.0557	0.6972	0.6225
0.156	0.4777	25.5996	1.3436	0.0541	0.6972	0.3871
$8 * 10^{-4}$	0.4777	25.6527	1.3295	0.0562	0.707	0.3716
$9.7 * 10^{-4}$	0.4777	25.6455	1.5202	0.0493	0.7071	0.0783

The diameter increases with decreasing $\partial_{rat}^{min}(1)$ values but the relative diameter of high amplitude points decreases. Note that the entropy of high amplitude points is lying at around 70% of the maximum value which is much larger than we would expect, but the minimum ratio distances are very low ($\approx 5\%$ of the maximum value).

Also note the large diameter but very low relative diameter of the high amplitude points in the last row. The corresponding plots for this simulation are given in figure 21.

Figure 21: Square Snowflake: Random Walk Simulation node 2415
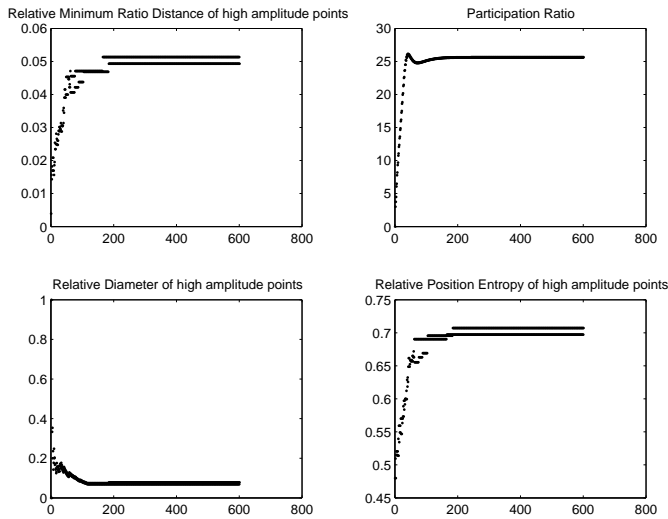
At a time step of about 200, D_{ha}^{rel} and S_{ha}^{rel} start jumping between two values; an indication of localization?

Table 4: **Square Snowflake** ($S(1)$ decreases)						

$\partial_{rel}(1)$	$S_{rel}(1)$	$PR(\infty)$	$DIAM(\infty)$	$D_{ha}^{rel}(\infty)$	$S_{ha}^{rel}(\infty)$	$DIAM_{ha}^{rel}(\infty)$
0.314	0.1464	25.5997	0.9071	0.0557	0.6972	0.6225
0.3436	0.07	25.6456	0.888	0.0566	0.7071	0.6483
0.3572	0.058	25.5997	1.1761	0.0575	0.6972	0.2941
0.4572	$8.21 * 10^{-3}$	25.6456	0.9254	0.0559	0.707	0.5829
0.492	$1.78 * 10^{-3}$	25.6456	0.9135	0.0559	0.7071	0.6047
0.492	$1.52 * 10^{-3}$	25.6005	0.9209	0.0568	0.6972	0.5998

The diameter of high amplitude points is large and does not decrease with decreasing entropy values. Here, row 3 sticks out with a relatively low $DIAM_{ha}^{rel}(\infty)$ value. The corresponding plots are given in figure 22.

Figure 22: Square Snowflake: Random Walk Simulation node 824
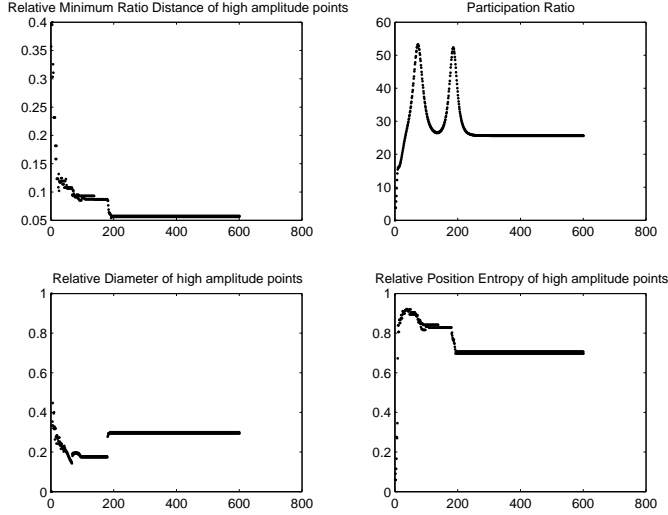
In both tables, $D_{ha}^{rel}(\infty)$ and $S_{ha}^{rel}(\infty)$ show little fluctuations.

Table 5: **Triadic Snowflake** ($\partial_{rat}^{min}(1)$ decreases)						
$\partial_{rel}(1)$	$S_{rel}(1)$	$PR(\infty)$	$DIAM(\infty)$	$D_{ha}^{rel}(\infty)$	$S_{ha}^{rel}(\infty)$	$DIAM_{ha}^{rel}(\infty)$
0.4776	0.063	156.8692	0.5492	0.0153	0.4897	0.7333
0.3973	0.231	169.2816	0.7011	0.0144	0.4883	0.5033
0.0206	0.4579	221.154	0.9773	0.0231	0.5247	0.1822
0.0163	0.4663	86.536	0.011	0.0147	0.4897	0.1895
0.0617	0.4285	221.3947	0.9558	0.023	0.5246	0.1944
$1.13 * 10^{-3}$	0.4201	222.6706	1.0908	0.0308	0.5301	0.187

In contrast with what was observed for the square domain, we see here in table 5 different participation ratios for different starting nodes. Note that on the triadic domain the entropy of high amplitude points are lying at only about 50%, as opposed to about 70% on the other domain. As observed on the square domain, $DIAM_{ha}^{rel}$ drops with decreasing $\partial_{rat}^{min}(1)$. This is not the case when we decrease $S(1)$, as shown in table 6.

Table 6: **Triadic Snowflake** ($S(1)$ decreases)						
$\partial_{rel}(1)$	$S_{rel}(1)$	$PR(\infty)$	$DIAM(\infty)$	$D_{ha}^{rel}(\infty)$	$S_{ha}^{rel}(\infty)$	$DIAM_{ha}^{rel}(\infty)$
$6.25 * 10^{-4}$	0.4277	214.5546	1.112	0.0348	0.5263	0.1964
0.3973	0.231	169.2816	0.7011	0.0144	0.4883	0.5033
0.4776	0.063	156.8692	0.5492	0.0153	0.4897	0.7333
0.4752	0.063	319.6411	0.5881	0.0163	0.4897	0.7852
0.4895	0.05	222.6769	0.5999	0.025	0.5310	0.6707
0.4969	0.042	222.6763	0.6102	0.025	0.531	0.6707

Unlike in the case of the square Snowflake, we notice here that a decrease in the initial node entropy results in a decrease in $DIAM(\infty)$.

We next present in tables 7 and 8 some random walks started at high entropy/high ∂_{rat}^{min} nodes on both domains. We point out that on both domains, no node with $\partial_{rat}^{min}(1)$ and $S(1)$ greater than $1/2$ of their respective maximum values exists.

Table 7: **Square Snowflake**

$\partial_{rel}(1)$	$S_{rel}(1)$	$PR(\infty)$	$DIAM(\infty)$	$D_{ha}^{rel}(\infty)$	$S_{ha}^{rel}(\infty)$	$DIAM_{ha}^{rel}(\infty)$
0.7109	0.3328	25.6465	1.2798	0.0644	0.707	0.2032
0.7108	0.3312	25.5997	1.2847	0.065	0.6972	0.1961
0.5625	0.3394	25.762	0.9719	0.0548	0.7071	0.5256
0.5624	0.3375	25.7173	0.9733	0.0563	0.6972	0.5315
0.3332	0.5414	26.6456	1.2564	0.0538	0.7071	0.2661
0.3125	0.4227	25.5996	1.0088	0.0796	0.6972	0.4651

Entropy values of high amplitude points are the same as for starting nodes with low $\partial_{rat}^{min}(1)$ and $S(1)$ values. $DIAM_{ha}^{rel}(\infty)$ varies a lot.

Table 8: **Triadic Snowflake**

$\partial_{rel}(1)$	$S_{rel}(1)$	$PR(\infty)$	$DIAM(\infty)$	$D_{ha}^{rel}(\infty)$	$S_{ha}^{rel}(\infty)$	$DIAM_{ha}^{rel}(\infty)$
0.575	0.0113	211.4606	0.8316	0.0229	0.5256	0.275
0.527	0.3067	222.0036	0.7875	0.0236	0.5265	0.3438
0.4994	0.4138	222.0426	0.8087	0.0236	0.5265	0.3155
0.4598	0.5141	222.0645	0.8299	0.0236	0.5265	0.2896
0.3065	0.743	86.2551	0.9098	0.0151	0.4939	0.1511
0.3248	0.5546	87.0524	0.8781	0.026	0.4896	0.1892

$DIAM_{ha}^{rel}(\infty)$ values are lower than on the square domain. $DIAM(\infty)$ also seems to be lower and $D_{ha}^{rel}(\infty)$ only lies at about 2% of the maximum value instead of at about 5.5% on the other domain. Again, participation ratios vary on the triadic domain while they are constant for the square Snowflake.

Tables 9 and 10 refer to the simulations run with high $\partial_{rat}^{min}(1)$ and low $S(1)$ values.

Table 9: **Square Snowflake**

$\partial_{rel}(1)$	$S_{rel}(1)$	$PR(\infty)$	$DIAM(\infty)$	$D_{ha}^{rel}(\infty)$	$S_{ha}^{rel}(\infty)$	$DIAM_{ha}^{rel}(\infty)$
0.7656	$1.31 * 10^{-8}$	25.5997	1.2649	0.0683	0.6972	0.2045
0.9376	$6.49 * 10^{-5}$	25.6468	0.8764	0.0548	0.7071	0.6714
0.9376	$2.96 * 10^{-4}$	25.6473	0.9209	0.0592	0.7071	0.596
0.9376	$2.1 * 10^{-9}$	25.6053	0.8643	0.0501	0.6972	0.702
0.2188	$4.07 * 10^{-12}$	25.6595	0.925	0.0533	0.7071	0.5922
0.9376	$6.49 * 10^{-5}$	25.5997	0.8796	0.0563	0.6972	0.6725

Table 10: **Triadic Snowflake**

$\partial_{rel}(1)$	$S_{rel}(1)$	$PR(\infty)$	$DIAM(\infty)$	$D_{ha}^{rel}(\infty)$	$S_{ha}^{rel}(\infty)$	$DIAM_{ha}^{rel}(\infty)$
0.4952	0.04	222.6771	0.6844	0.025	0.531	0.4638
0.59	$4.32 * 10^{-3}$	221.6813	0.6529	0.0182	0.5228	0.5147
0.6383	0.6554	222.6791	0.7485	0.0253	0.5324	0.3408
0.734	0.147	210.968	0.747	0.0219	0.524	0.3908
0.772	0.1176	213.7942	0.7185	0.0224	0.5255	0.4135
0.8483	$1.05 * 10^{-6}$	211.4231	0.717	0.0229	0.5256	0.3808

Note that low $S(1)$ values are not sufficient for $DIAM_{ha}^{rel}(\infty)$ values to drop.

Finally, tables 11 and 12 provide the results of the simulations run with low $\partial_{rat}^{min}(1)$ and high $S(1)$ values.

Table 11: **Square Snowflake**

$\partial_{rel}(1)$	$S_{rel}(1)$	$PR(\infty)$	$DIAM(\infty)$	$D_{ha}^{rel}(\infty)$	$S_{ha}^{rel}(\infty)$	$DIAM_{ha}^{rel}(\infty)$
0.1876	0.9554	25.5997	1.3179	0.0624	0.697	0.1221
0.1388	0.949	25.6047	0.9904	0.0563	0.6972	0.5015
0.0936	0.9363	25.5997	1.3681	0.0692	0.6972	0.087
0.09	0.9358	25.6455	1.3514	0.0548	0.7071	0.0842
0.078	0.9044	25.6456	1.3486	0.0548	0.7071	0.0882
0.078	0.9044	25.5996	1.3208	0.0579	0.6972	0.1165

Note the high and low values of the relative diameter of high amplitude points of row 2 an 3, respectively.

Table 12: **Triadic Snowflake**

$\partial_{rel}(1)$	$S_{rel}(1)$	$PR(\infty)$	$DIAM(\infty)$	$D_{ha}^{rel}(\infty)$	$S_{ha}^{rel}(\infty)$	$DIAM_{ha}^{rel}(\infty)$
0.206	0.7478	86.5501	0.8474	0.0292	0.4897	0.2385
0.1618	0.9957	86.6407	0.8497	0.0313	0.4897	0.2546
0.1147	0.8944	222.1414	0.8283	0.0238	0.5282	0.3386
0.09	0.8361	213.3961	0.8561	0.0236	0.5254	0.1841
0.082	0.7879	86.8069	0.8565	0.0312	0.4897	0.275
0.061	0.7016	213.8787	0.9734	0.0233	0.5243	0.121

Even though we start in a high entropy region, it seems to be sufficient to have low $\partial_{rel}(1)$ for a drop in $DIAM_{ha}^{rel}(\infty)$ to occur.

7 Results and Discussion

Our numerical calculations show the following results on both domains:

- All five quantities of interest approach an asymptotic limit.

- $D_{ha}^{rel}(\infty)$ and $S_{ha}^{rel}(\infty)$ are independent of the starting node. Values lie at about 5.5% and 70% of the respective maximum values on the square Snowflake and at about 2.5% and 50% of the respective maximum values on the triadic Snowflake.

- The asymptotic limit of the Diameter $(DIAM(\infty))$ varies a lot within a region but overall seems to be a little lower when walks are started in low distance/low entropy regions.

- When $S(1)$ and $\partial_{rat}^{min}(1)$ are very low, the diameter of high amplitude points $(DIAM_{ha}^{rel}(\infty))$ is significantly smaller than for walks started in any other region.

- No node with $S(1)$ and $\partial_{rat}^{min}(1)$ values larger than half their respective maximum values can be found.

Comparing results on the triadic and square domains, we observe the following:

- Astonishingly, the participation ratio of the square Snowflake is approximately the same for any starting node. On the triadic domain, we find three different approximate values: even if $S(1)$ and $\partial_{rat}^{min}(1)$ values are similar (row three and four in table 6), we can observe different participation ratios.

- The participation ratio on the triadic Snowflake is higher than on the square Snowflake: On the square domain the participation ratio lies at 0.5%, the three values on the triadic domain correspond to about 1, 3 and 4% of the total number of nodes in the discretization.

- On the triadic domain, no node with $\partial_{rat}^{min} < \frac{1}{2} \max\left(\partial_{rat}^{min}\right)$ and $S < \frac{1}{24} \max\left(S\right)$ can be found, while on the square domain, we can find a node satisfying $S < \frac{1}{251} \max\left(S\right)$ for $\partial_{rat}^{min} < \frac{1}{2} \max\left(\partial_{rat}^{min}\right)$.

- The minimum ratio distances of high entropy points on the square domain are constant and lie at about 5% of its maximum value on the domain. On the triadic Snowflake, minimum ratio distances of high entropy points vary: we find values from 1% to 3% of the maximum. These seem to be independent of where the starting node lies.

- For both domains, the $S_{ha}^{rel}(\infty)$ values do not show sensitivity to initial conditions. It is rather surprising, though, that they are larger on the square Snowflake.

In summary, we can say that random walks started at low ∂_{rat}^{min} nodes show localization in the form of decreased diameter of high amplitude points. This localization occurs on both domains with the same frequency. The value of the initial node entropy does not seem to have a great influence on the dynamics of the system: a decrease does not necessarily result in a decrease of the diameter of high amplitude points. $D_{ha}^{rel}(\infty)$ and $S_{ha}^{rel}(\infty)$ always level off to about the same value on both domains, with the $D_{ha}^{rel}(\infty)$ very low and $S_{ha}^{rel}(\infty)$ values relatively large. This is a little surprising and requires further investigation. The main result of the numerical simulations is that the dynamics of the two systems are very similar. Hence, we can not conclude that narrow channels in the geometry of the square domain cause localization of the Dirichlet eigenfunctions. But there certainly are noticeable geometric differences on the two domains. The nodal entropies found on the square Snowflake are significantly higher. Maybe the greater diversity in $\partial_{rat}^{min}(1)$ distribution on this domain is the cause for localization found in some of the Dirichlet eigenfunctions. This hypothesis should be further investigated. One should create weighted graphs with different nodal entropy distributions and test how the dynamics of the system is influenced. Another direction of further research in this area would be to conduct a thorough analysis of the transfer matrix $\mathbf{T}$. It would be interesting to determine if the nature of the eigenvalues and eigenfunctions of $\mathbf{T}$ reveals information about the course taken by a random walker.

References

[At]   K. E. Atkinson, *An Introduction to Numerical Analysis*, 2nd edn., John Wiley and Sons, New York (1989)

[BeDe] R. J. Bell and P. Dean, *Atomic vibrationsin vitreous silica*, Disc. Faraday Soc. **50** (1970), 55-61

[Be1]   M. V. Berry, *Distribution of modes in fractal resonators*, in: Structral Stability in Physics (W. Güttinger, and H. Eikemeier, eds.), Springer-Verlag, Berlin (1979), pp. 51-53

[Be2]   M. V. Berry, *Some geometric aspects of wave motion: Wavefront dislocations, diffraction catatrophes, diffractals*, in: Geometry of the Laplace Operator, Proc. Sympos. Pure Math., vol. 36, Amer. Math. Soc., Providence, R. I. (1980), pp. 13-38

[BroCa] J. Brossard and R. Carmona, Can one hear the dimension of a fractal?, *Commun. Math. Phys.* **104** (1986), 103-122

[Ev]   L. C. Evans, *Partial Differential Equations*, Graduate Studies in Mathematics, vol. 19, Amer. Math. Soc., Providence, R. I. (1998)

[EveRRPS] C. Even, S. Russ, V. Repain, P. Pieranski and B. Sapoval, *Localization in fractal drums: An experimental study*, Phys. Rev. Lett. **83** (1999), 726-729

[F]   K. J. Falconer, *Fractal Geometry: Mathematical Foundations and Applications*, John Wiley and Sons, London (1990)

[Ha]   M. J. W. Hall, *Universal geometric approach to uncertainty, entropy and information*, Phys. Rev. A **50** (1999), 2602-2615

[IK]   E. Isaacson and H. Keller, *Analysis of Numerical Methods*, John Wiley and Sons, New York (1966)

[L1]   M. L. Lapidus, Fractal drum, inverse spectral problems for elliptic operators and a partial resolution of the Weyl–Berry conjecture, *Trans. Amer. Math. Soc.* **325** (1991), 465-529

[L2]   M. L. Lapidus, *Spectral and fractal geometry: From the Weyl–Berry conjecture for the vibrations of fractal dums to the Riemann zeta-function,* in: Differential Equations and Mathematical Physics (C. Bennewitz, ed.), Proc. Fourth UAB Internat. Conf. (Birmingham, March 1990), Academic Press, New York, 1992, pp. 151-182

[L3]   M. L. Lapidus, *Vibrations of fractal drums, the Riemann hypothesis, waves in fractal media, and the Weyl–Berry conjecture,* in: Ordinary and Partial Differential Equations (B. D. Sleeman and R. J. Jarvis, eds.), vol. IV, Proc. Twelfth Internat. Conf. (Dundee, Scotland, UK, June 1992), Pitman Research Notes in Math. Series, vol. 289, Longman Scientific and Technical, London, 1993, pp. 126-209

[LP]   M. L. Lapidus and M. M. H. Pang, *Eigenfunctions of the Koch snowflake domain,* Commun. Math. Phys. **172** (1995), 359-376

[LNRG] M. L. Lapidus, J. W. Neuberger, R. J. Renka and C. A. Griffith, *Snowflake harmonics and computer graphics: Numerical computation of spectra on fractal drums,* Internat. J. Bifurcation & Chaos **6** (1996), 1185-1210

[Sa1] B. Sapoval, *Fractals,* Bernard Aumont, Aditech, Paris (1990)

[Sa2] B. Sapoval, *Experimental observation of local modes in fractal drums,* Physica D **38** (1989), 296-298

[SG]   B. Sapoval and T. Gobron, *Vibrations of strongly irregular or fractal resonators,* Phys. Rev. E **47** (1993), 3013-3024

[SGM] B. Sapoval, T. Gobron and A. Margolina, *Vibrations of fractal drums,* Phys. Rev. Lett. **67** (1991), 2974-2977

[Si]   I. Simonsen, *Diffusion and networks: A powerful combination!*, Physica A **357** (2005), 317-330

[SiErMaSn] I. Simonsen, K. A. Eriksen, S. Maslov and K. Sneppen, *Diffusion on complex networks: A way to probe their large-scale topological structures*, Physica A **336** (2004), 163-173

[Th]   D. J. Thouless, *Electrons in disordered systems and the theory of localization*, Phys. Rep. **13** (1974), 93-142

[We]   F. Wegner, *Bounds on the density of states in disordered systems*, Z. Phys. B **44** (1981), 9-15